

## Electronic Structure, Electronic Charge Density and Optical Properties Analyses of $\text{Rb}_2\text{Al}_2\text{B}_2\text{O}_7$ Compound: DFT Calculation

A. H. Reshak<sup>1,2</sup>, Z. A. Alahmed<sup>3</sup>, Sikander Azam<sup>1,\*</sup>

<sup>1</sup>New Technologies - Research Center, University of West Bohemia, Univerzitni 8, Pilsen 306 14, Czech Republic

<sup>2</sup>Center of Excellence Geopolymer and Green Technology, School of Material Engineering, University Malaysia Perlis, 01007 Kangar, Perlis, Malaysia

<sup>3</sup>Department of Physics and Astronomy, King Saud University, Riyadh 11451, Saudi Arabia

\*E-mail: [sikander.physicst@gmail.com](mailto:sikander.physicst@gmail.com)

Received: 18 August 2013 / Accepted: 14 October 2013 / Published: 8 December 2013

---

We have presented an analysis of some important electronic and optical characteristics of the  $\text{Rb}_2\text{Al}_2\text{B}_2\text{O}_7$  compound, based on the ab initio calculations of its electronic band structure, electronic charge density and dielectric tensor function. The band gap is found to be indirect of about 4.156, 4.471 and 5.205 eV for LDA, GGA and EVGGA respectively. The contributions to the top of valence band and bottom of conduction band come predominantly from O s/p, Al s/p and Rb s/p states, respectively. The distribution of the total electronic charge density maps (in the units of e/a.u.<sup>3</sup>) has been calculated along the (101) plane. The optical absorption spectrum is calculated and interpreted in terms of electronic band structure for incident radiation energy up to 14 eV. The principal absorption occurs within the energy range from 6.0 to 14.0 eV, originating mainly from the electronic transitions from the O-s to Al-s/p states. The complex dielectric function, refractive index, birefringence, energy-loss spectrum and reflectivity have been calculated.

---

**Keywords:** electronic structure, electronic charge density and optical properties: DFT

### 1. INTRODUCTION

Oxide materials of the borate group have been the subject of increasing interest during the past years. A large number of papers dealing with the synthesis, crystal growth and properties of new borates as well as borate crystal chemistry have appeared in the literature. The nonlinear optical borate crystals are the fundamental materials for applications in high-power frequency conversion and laser systems because of appropriate nonlinear optical coefficients, reasonable birefringence, wide transparency range including UV range and very high optical damage thresholds [1-5]. Advanced

crystal growth technology has made borate crystals available on industrial scale with large dimensions and great optical quality [6-10]. Researchers are investigating borates compounds as prospective photonic and nano-technology materials due to electronic, chemical and luminescent properties [11-19].

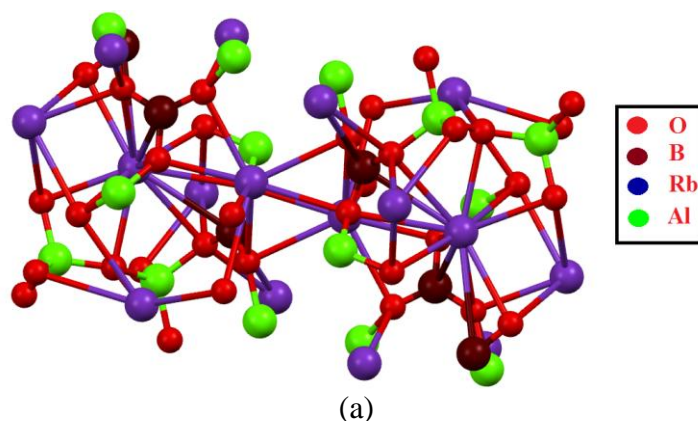
This interest is due, above all, to the excellent non-linear optical (NLO) and/or lasing properties of the crystals of some borates. The unique structure characteristics of the boron–oxygen groups in a series of these compounds determine their enhanced UV transparency, good non-linearity and relatively high resistance against laser-induced damage.

On the other hand, the extraordinary versatility of borate structures facilitates the design of new compounds with appropriate optical properties. Potassium aluminum borate  $K_2Al_2B_2O_7$  (KABO), is amongst the best borate crystals pertinent to optical frequency exchange in ultraviolet (UV) spectral range [20–24]. To improve its applications in the optoelectronic devices, the ionic engineering is required to amend the electronic, vibrational and optical properties in KABO. Wide-range element substitution is possible at  $K^+$  and  $Al^{3+}$  sites in KABO crystal lattice, and several compounds and solid solutions related to KABO family were observed in the past [25–29]. Recently at room temperature as  $x \sim 0.75$ , a solid solution  $K_{2(1-x)}Rb_{2x}Al_2B_2O_7$  has been discovered [30]. Though for  $K_{2(1-x)}Rb_{2x}Al_2B_2O_7$  solid solutions, only structural properties were obtained in [30] for numerous compositions. Recently Atuchin et al. [31] studied the physical properties and the vibrational parameters of  $KRbAl_2B_2O_7$  (KRABO) borate, using Raman spectroscopy, X-ray photoelectron spectroscopy and the pseudo-potential CASTEP package.

From above we notice that there is no comprehensive research work neither experimental nor theoretical has been done on such important compound. Therefore, we thought it would be worthwhile to perform a comprehensive theoretical work based on full potential density functional theory, to investigate the electronic band structure, total and partial density of states, the distribution of the total electronic charge density, and the optical properties of KRABO.

## 2. CALCULATION DETAILS AND STRUCTURE OPTIMIZATION

We make used of the crystallographic data of  $Rb_2Al_2B_2O_7$  compound, from the work L. Judith et. al. [40], the molecular and unit cell structure are shown in Fig. 1.



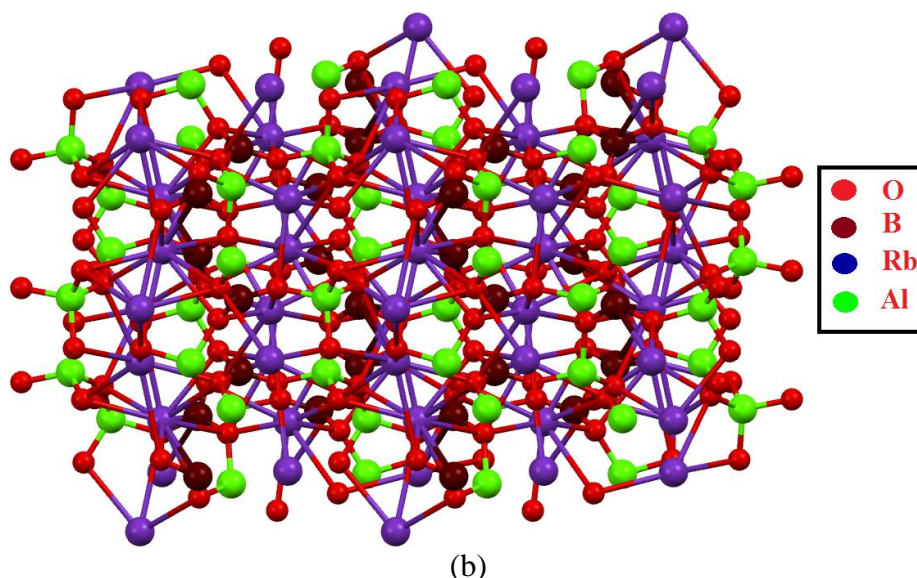


**Figure 1.** Molecular and unit cell structure for  $\text{Rb}_2\text{Al}_2\text{B}_2\text{O}_7$  compound.

The self-consistent calculations of  $\text{Rb}_2\text{Al}_2\text{B}_2\text{O}_7$  compound were performed using the density-functional theory (DFT) [32] based on full potential linear augmented plane wave (FP-LAPW) method [33] as incorporated in WIEN2k code [34]. In this process, the electronic wave functions, charge density and crystal potential were expanded in spherical harmonics inside the non-overlapping spheres centered at each nuclear position (atomic spheres with radii RMT), and in plane waves in the rest of the space (interstitial region). The choice for the atomic sphere radii (in atomic units) was 2.5 for Rb, 1.53 for Al and 1.21 for both B and O. Inside atomic spheres the partial waves were expanded up to  $l_{\text{max}} = 10$ , while the number of plane waves in the interstitial was limited by the cut-off at  $K_{\text{max}} = 7.0/\text{RMT}$ . The charge density was Fourier expanded up to  $G_{\text{max}} = 12$ . Exchange and correlation effects were treated by local density approximation (LDA), generalized-gradient approximation (GGA) and Engle-Vosko GGA [35-38]. We have optimized the atomic positions taken from XRD data by minimization of the forces acting on the atoms. From the relaxed geometry the electronic structure, electronic charge density and the optical properties can be determined. The optimized geometry along with the experimental once [40] were listed in Table 1.

**Table 1.** Crystallographic parameters for  $\text{Rb}_2\text{Al}_2\text{B}_2\text{O}_7$  compound.

Space group number 14						
Symmetry space group name 'P 1 21/c 1'						
Cell Angle ( $^\circ$ )						
$\alpha = 90, \beta = 103.970, \gamma = 90$						
Cell length ( $\text{Å}$ )						
$a = 8.901, b = 7.5390, c = 11.905$						
Atoms	Exp. X	Opt. X	Exp. Y	Opt. Y	Exp. Z	Opt. Z

Rb1	0.03371	0.03536	0.14003	0.13915	0.62650	0.62741
Rb2	0.45632	0.45694	-0.13338	0.86738	0.85435	0.85320
Al1	-0.34247	0.65621	-0.12434	0.87479	0.62207	0.62173
Al2	-0.18525	0.81433	0.08342	0.08197	0.86588	0.86532
B1	0.15520	0.15636	0.08730	0.08699	0.91140	0.91076
B2	0.31910	0.31604	-0.11470	0.88473	0.56340	0.56135
O1	-0.20270	0.80065	0.18920	0.19066	0.39530	0.39680
O2	-0.30840	0.68867	0.01990	0.02092	0.73700	0.73681
O3	0.00640	0.00628	0.04070	0.03854	0.86200	0.86152
O4	0.46310	0.46063	-0.18940	0.81040	0.58920	0.58698
O5	0.28280	0.28018	0.03240	0.03319	0.49620	0.49442
O6	0.23730	0.23699	0.17900	0.17797	0.84550	0.84402
O7	-0.22940	0.76854	0.53810	0.53944	0.47950	0.47907

The optical response of the  $\text{Rb}_2\text{Al}_2\text{B}_2\text{O}_7$  compound was determined by calculating its complex dielectric tensor  $\varepsilon$ . Imaginary part of this tensor is proportional to the optical absorption spectrum of the material. It can be computed from knowledge of the electronic band structure. In the limit of linear optics, neglecting electron polarization effects and within the frame of random phase approximation, the expression for the imaginary part of  $\varepsilon$  is the following [39]:

$$\text{Im}\varepsilon_{\alpha\beta}(\omega) = \frac{4\pi^2 e^2}{m^2 \omega^2} \sum_{i,f} \int_{BZ} \frac{2dk}{2\pi^3} \langle \varphi_{fk} | P_{\beta} | \varphi_{ik} \rangle \cdot \delta(E_f(k)) - E_i(k) - \hbar\omega$$

For a vertical transition from a filled initial state  $|\varphi_{ik}\rangle$  of energy  $E_i(k)$  to an empty final state  $|\varphi_{fk}\rangle$  of energy  $E_f(k)$  with the same wave vector  $k$ .  $\omega$  is the frequency of the incident radiation,  $m$  the electron mass,  $P$  the momentum operator, and  $\alpha$  and  $\beta$  stand for the projections  $x$ ,  $y$ ,  $z$ .

The crystal structure of the  $\text{Rb}_2\text{Al}_2\text{B}_2\text{O}_7$  exhibits a monoclinic symmetry, space group # 14. The monoclinic symmetry has five nonzero components of the second-order dielectric tensor. In regardless of this only  $\varepsilon_2^{xx}(\omega)$ ,  $\varepsilon_2^{yy}(\omega)$  and  $\varepsilon_2^{zz}(\omega)$  are major, these are the imaginary parts of the frequency-dependent dielectric function. The resulting inter-atomic distances B–O, Al–O and Rb–O and also the calculated angles are shown in Table 2 which are in good agreement with the experimental data [40]. Each Rb and B atom is surrounded by four and three oxygen atoms at different distances.

**Table 2.** Calculated bond lengths and angles for  $\text{Rb}_2\text{Al}_2\text{B}_2\text{O}_7$  compound

Bond	Exp. (Distance(Å))	Opt. (Distance(Å))
Rb1- O6	2.808 (2)	2.778
Rb1- O1	2.946 (3)	2.932
Rb1- O3	2.968 (3)	2.959
Rb1- O3	3.048 (3)	3.040
Rb1- O1	3.056 (3)	3.046
Rb1-O5	3.105 (3)	3.091
Rb1- O5	3.126 (3)	3.116
Rb2- O7	2.924 (3)	2.902
Rb2- O2	3.009 (3)	2.996
Rb2- O6	3.043 (3)	3.037
Rb2- O4	3.086 (3)	3.082

Rb2- O4	3.200 (3)	3.199
Rb2- O1	3.297 (3)	3.296
Rb2- O7	3.405 (3)	3.410
Rb2- O4	3.455 (3)	3.456
Al1- O2	1.716 (3)	1.725
Al1- O6	1.746 (3)	1.756
Al1- O4	1.749 (3)	1.758
Al1- O5	1.762 (3)	1.758
Al2- O2	1.725 (3)	1.716
Al2- O3	1.747 (3)	1.750
Al2- O7	1.755 (3)	1.762
Al2- O1	1.764 (3)	1.765
O3- B1	1.360 (5)	1.372
O6- B1	1.380 (5)	1.376
O7- B1	1.359 (5)	1.368
O1- B2	1.370 (5)	1.378
O4- B2	1.366 (5)	1.369
O5- B2	1.360 (5)	1.366
Bond	Exp. (Angle (°))	Opt.(Angle (°))
O2- Al- O6	112.30 (13)	112.17
O2- Al1- O4	109.32 (14)	109.23
O6- Al1- O4	105.08 (14)	105.73
O2- Al1- O5	111.00 (15)	110.38
O6- Al1- O5	105.17 (14)	104.88
O4- Al1- O5	113.82 (14)	114.36
O2- Al2- O3	109.87 (14)	110.78
O2- Al2- O7	109.16 (15)	108.80
O3- Al2- O7	109.03 (14)	109.33
O2- Al2- O1	112.30 (13)	112.59
O3- Al2- O1	108.52 (13)	107.75
O7- Al2- O1	107.89 (14)	107.50
O7- B1- O3	122.8 (4)	122.66
O7- B1- O6	118.6 (3)	118.81
O3- B1- O6	118.5 (3)	118.41
O5- B2- O4	123.0 (4)	122.69
O5- B2- O1	116.9 (3)	117.27
O4- B2- O1	120.0 (3)	120.04
Al1- O2- Al2	146.85 (18)	145.28

### 3. RESULTS AND DISSCUSION

#### 3.1. Electronic structure

The electronic band structures of the monoclinic  $\text{Rb}_2\text{Al}_2\text{B}_2\text{O}_7$  are calculated within LDA, GGA and EV-GGA schemes. In all cases the valence band maximum (VBM) is located at Y and the conduction band minimum (CBM) is located at  $\Gamma$  point, resulting an indirect energy band gap. The calculated electronic band structure profiles using these three schemes exhibiting different values of

the band gaps which is higher for EV-GGA. The calculated band gap is found to be 4.156, 4.471 and 5.205 eV for LDA, GGA and EVGGA respectively. In Fig. 2, we show the electronic band dispersion curves along some high symmetry directions of the Brillion zone of  $\text{Rb}_2\text{Al}_2\text{B}_2\text{O}_7$  compound for the EVGGA. Since EVGGA exhibit better band splitting than LDA and GGA, we therefore, show only the EVGGA results. In order to illuminate the nature of the electronic band structures, we have calculated the total and partial densities of states (TDOS and PDOS). These are presented in Fig. 3. The bands in the lower energy part (-10.0 and -5.0 eV) are dominated by the Rb-p, Al-s/p and O-s states with small contribution of B-s/p and O-p. The top of the valence band (-5.0 and 0.0 eV) is formed mainly from O-s/p and Al-s/p states with minimum contribution of B-p and Rb-s states.

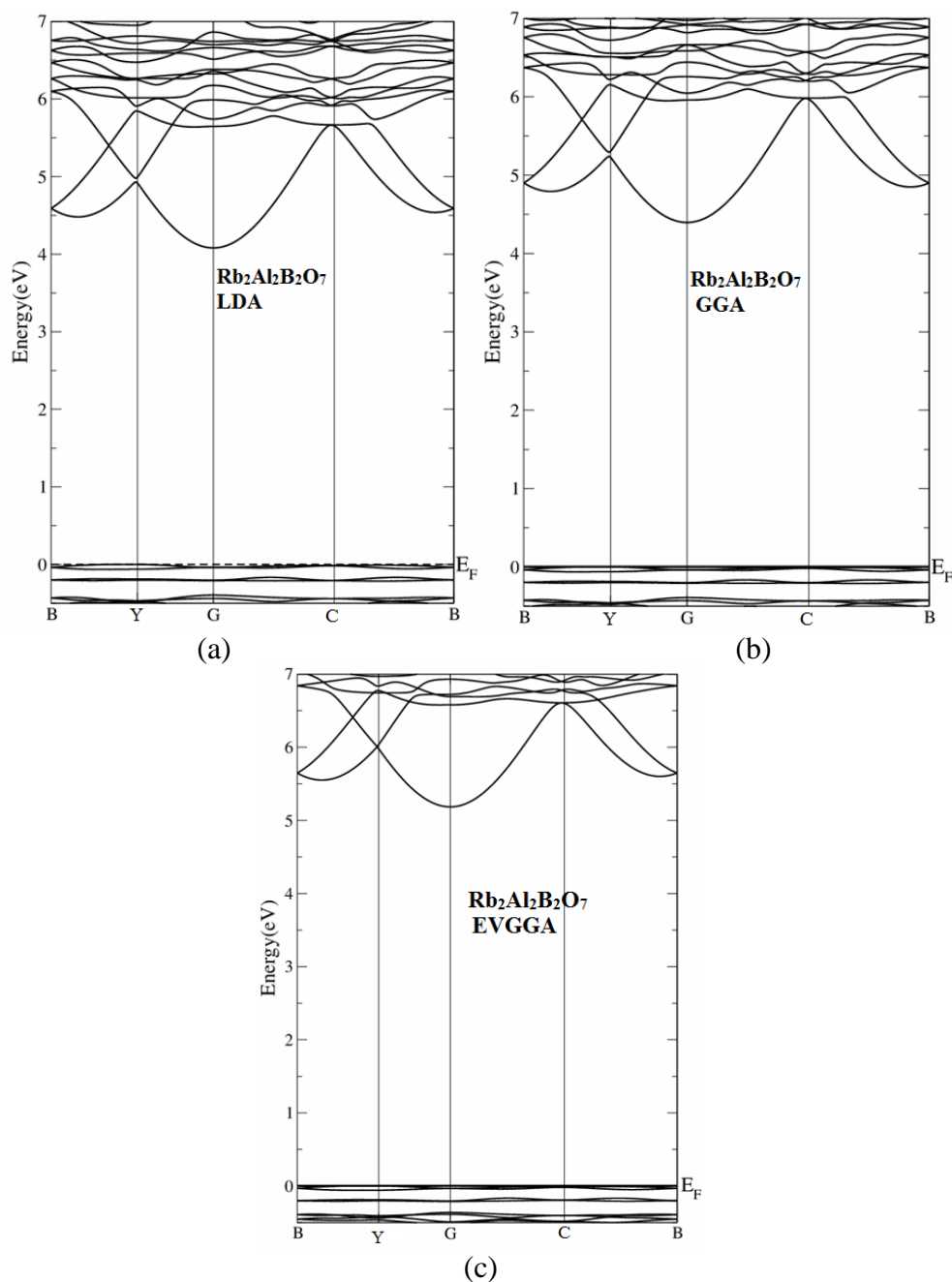
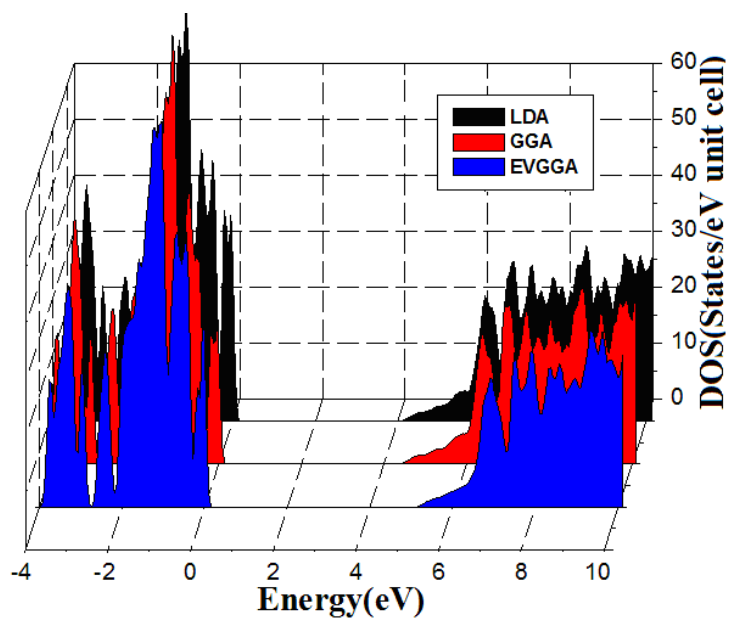
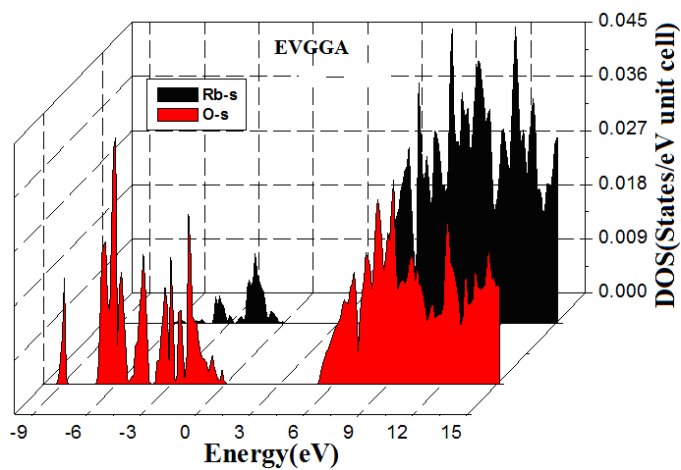


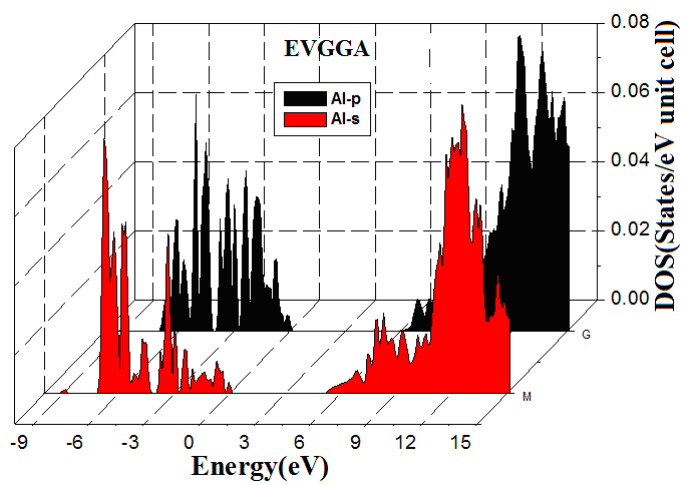
**Figure 2.** Calculated band structures for LDA, GGA and EVGGA for  $\text{Rb}_2\text{Al}_2\text{B}_2\text{O}_7$  compound.



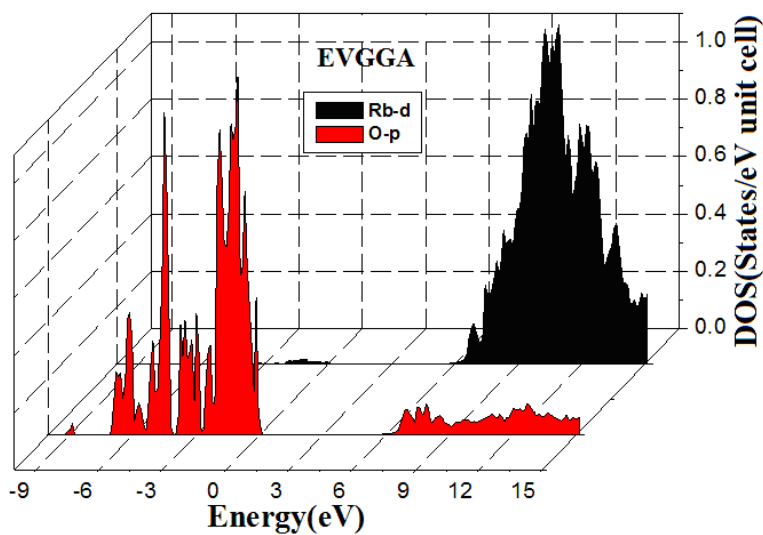
(a)



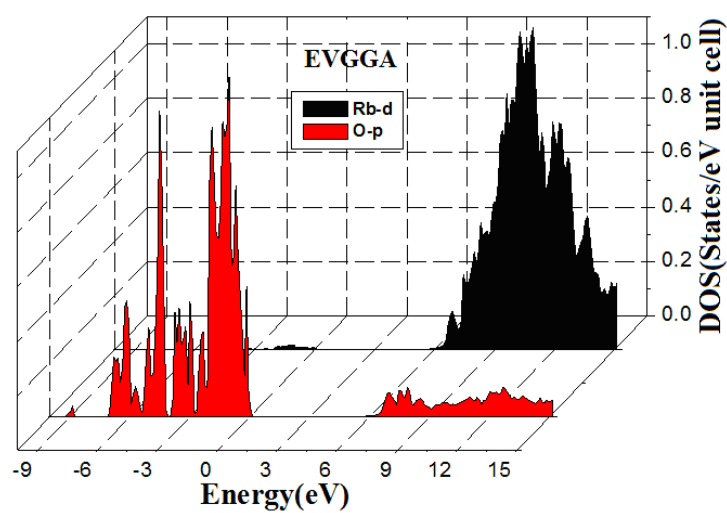
(b)



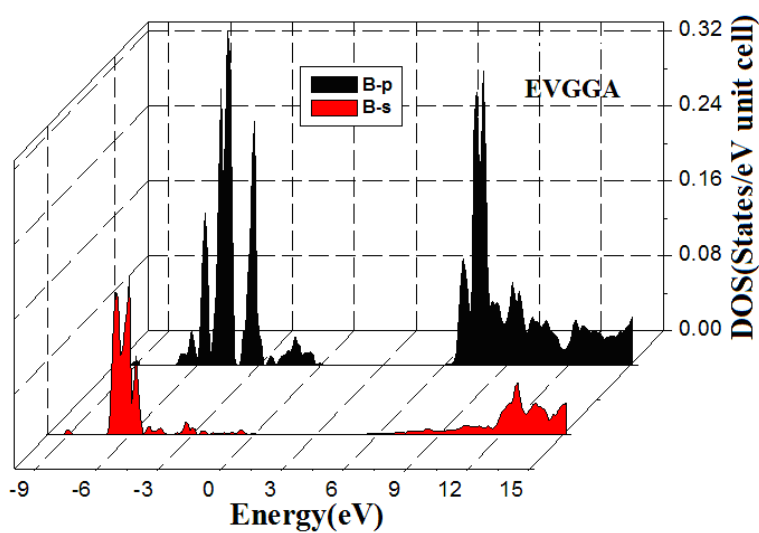
(c)



(d)



(e)



(f)

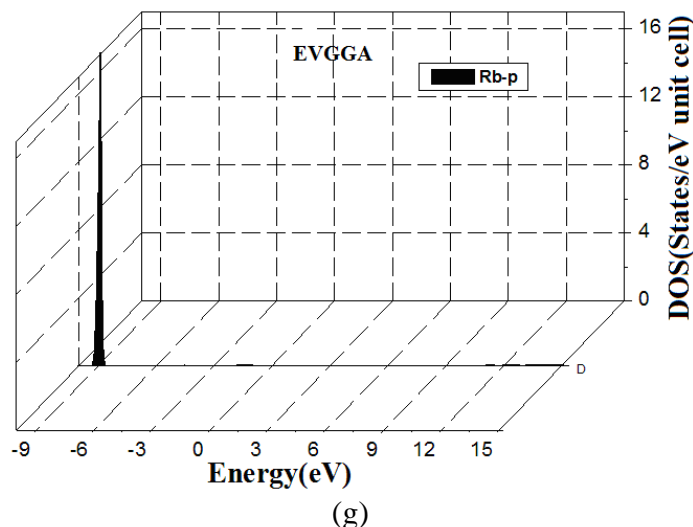


**Figure 3.** Calculated total and partial densities of states for Rb<sub>2</sub>Al<sub>2</sub>B<sub>2</sub>O<sub>7</sub> compound (State/eV unit cell)

In the conduction band the lower energy one (5.2 and 10.0 eV) accommodates mostly the Rb-s/d and O-s states with small contribution of O-p, B-p and Al-s/p. While the upper part (10.0 and 14.0 eV) is composed of the Rb-s/d, Al-s/p and O-s states with small admixture of B-p states. In the conduction band the lower energy part (above 7 eV) consists of the hybridized Rb-s and O-s states. While in the valance band (-7.0 and -4.0 eV) consists of hybridized Al-s and Al-p, B-s and O-p, and B-p and O-p states.

### 3.2. Effective mass

The effective mass is a quantity that is utilized to simplify band structure by making a similarity to the performance of a free element with that mass. For some reasons and some materials, the productive mass can be considered to be a simple constant of a material. In general, although, the valve of effective mass depends on the purpose for which it is utilized, and can vary depending on a number of components. As it simplifies the more general band used, the electrical devices effective mass can be seen as a significant basic parameter that leverages discernable properties of a solid, encompassing everything from the efficiency of a solar cell to the pace of an integrated circuit.

The effective mass of electrons ( $m_e^*$ ) was calculated from the band structure of the Rb<sub>2</sub>Al<sub>2</sub>B<sub>2</sub>O<sub>7</sub> compound, this valve was estimated from the curvature of the conduction band minimum (band # 217). The diagonal elements of the effective mass tensor,  $m_e$ , for the electrons in the conduction band are calculated around  $\Gamma$  direction in k space using the following well-known relation:

$$\frac{1}{m_e^*} = \frac{1}{\hbar^2} \frac{\partial^2 E(k)}{\partial k^2} \dots \dots \dots (1)$$

The effective mass of electron is assessed by fitting the electronic band structure to a parabolic function Eq. (1). The calculated electron effective mass ratio ( $m_e^*/m_e$ ) for  $Rb_2Al_2B_2O_7$  compound around  $\Gamma$  is 0.092.

We also calculated the effective mass of the heavy holes around B direction and light holes around C for  $Rb_2Al_2B_2O_7$  compound, these values are 0.0728 and 0.5134.

### 3.3. Electronic charge density:

In order to understand the distribution of the total electronic charge density maps of  $Rb_2Al_2B_2O_7$  compound, the valence electronic charge density maps (in the units of  $e/a.u.^3$ ) have been depicted in Fig. 4 along (1 0 1) crystallographic plane. This figure demonstrates that there is no substantial charge density distributed between Rb atoms.

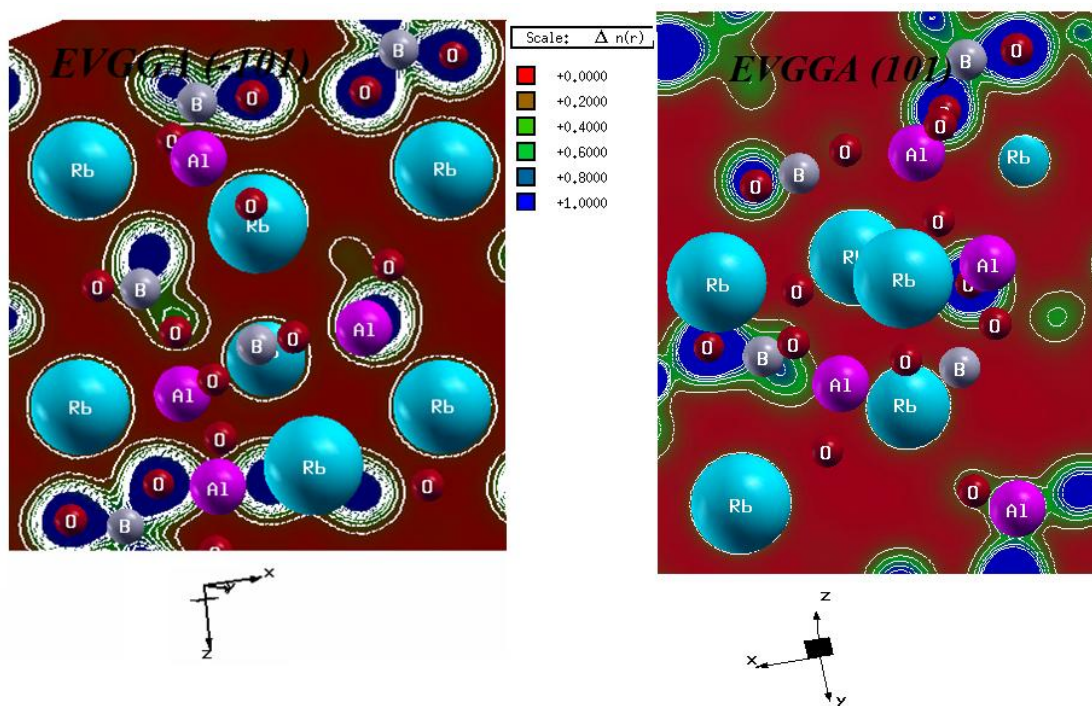


**Figure 4.** Calculated electronic charge density for  $Rb_2Al_2B_2O_7$  compound.

The bonding has a significant covalent character due to sharing of charge between O atoms. Moreover, the charge transfer occurs mainly from B and Al atoms towards O atom. It is clear that Rb and O atoms shows the ionic nature though the charge density contours around the oxygen is not completely circular but it shows the ionic bonding. The hump appears in the electronic charge density of oxygen atom, due to the high electro negativity which attracts the boron atom. We have also calculated the electronic charge density in the (-101) crystallographic plane in order to explore the anisotropy of the electronic charge density in the  $Rb_2Al_2B_2O_7$  compound. As it is clear from Fig. 4 that in (-101) crystallographic plane, B atom shows no charge density but as we move from the (-101)

plane to (101) plane there is the weak charge density. In the (101) plane the O atom shows the ionic nature but in the (-101) plane this ionic nature is absent and shows purely covalent bonding with the other O atom. In the (-101) the O-B makes the covalent bonding while this covalent bonding is absent in the (101) plane. As clear from the scale that the blue color show the greater charge density. So the oxygen atom has the greater charge density then the other atoms.

### 3.4. Optical properties

The complex dielectric function is directly related to the energy band structure of solids. The optical spectroscopy analysis of is a powerful tool to determine of the overall band behavior of a solid [41-43]. Therefore precise FPLAPW calculations are desirable to figure out the optical spectra.

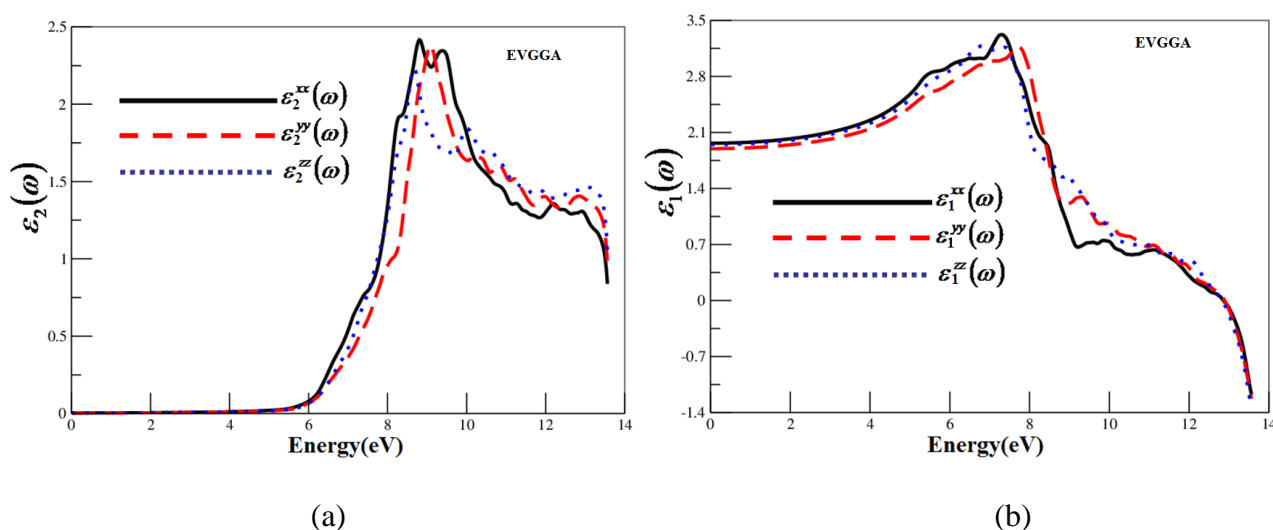


**Figure 5.** Calculated (a) imaginary and (b) real part of dielectric tensor function for Rb<sub>2</sub>Al<sub>2</sub>B<sub>2</sub>O<sub>7</sub> compounds  $\varepsilon_2(\omega)$  and  $\varepsilon_1(\omega)$ .

Fig. 5a and b, shows the spectrum of the real and imaginary parts of the complex dielectric function versus the photon energy. The interpretation of this spectrum in terms of electronic structure, presented in the Fig. 2, reveals the manner by which the compound absorbs the incident radiation. The lowest energy part of spectrum (from 5.5 to 10.0 eV) is characterized by two peaks of highest intensity. It is caused by electronic transitions from the top of valence band to the isolated low energy block in the conduction band. The first peak is generated mainly by transitions from the O-2p to the Rb-s states. The second peak is dominated by transitions from the O-2p to the Al-s. Knowing the imaginary part of the complex dielectric function we have calculated its real part (see Fig.5b) using Kramers–Kronig relations, and then computed various optical constants which characterize the propagation of the electromagnetic wave through the material [30]. The results of our calculated  $\varepsilon_2^{xx}(\omega)$ ,  $\varepsilon_2^{yy}(\omega)$  and  $\varepsilon_2^{zz}(\omega)$  are shown in Fig. 5a. The static real part (see Fig.5b) of dielectric function,  $\varepsilon_1(0)$ , along the three crystallographic directions is found to be 1.965 for  $\varepsilon^{xx}(0)$ , 1.897

for  $\epsilon^{yy}(0)$  and 1.947 for  $\epsilon^{zz}(0)$ . The uniaxial anisotropy  $\delta\epsilon = [(\epsilon_0^{\parallel} - \epsilon_0^{\perp}) / \epsilon_0^{\text{tot}}]$  is -0.00826 confirm the existence of the anisotropy in the  $\text{Rb}_2\text{Al}_2\text{B}_2\text{O}_7$  compound. The deviation in the values of static dielectric function indicates the anisotropic behavior of  $\text{Rb}_2\text{Al}_2\text{B}_2\text{O}_7$  compound. The other evaluated optical properties in which the most important constant is the refractive index, which is related with the linear electro-optical coefficient that in turn determines the photorefractive sensitivity of the  $\text{Rb}_2\text{Al}_2\text{B}_2\text{O}_7$  crystal. Fig. 6a, shows the variation of the calculated refractive index. It is seen that the refraction index reaches maximal values for the energies near the absorption threshold of the material (band gap energy). We also calculated the birefringence. Figure 6b shows the spectral comportment of the birefringence  $\Delta n(\omega)$  for the  $\text{Rb}_2\text{Al}_2\text{B}_2\text{O}_7$ . Birefringence is necessary only in the non-absorbing region, which is below the energy gap. The  $\Delta n(\omega)$  spectral reliance shows strong oscillations in the energy range from 5.0 eV up to 13.61 eV. We find that the static value of the birefringence  $\Delta n(0)$  equal to -0.00403.

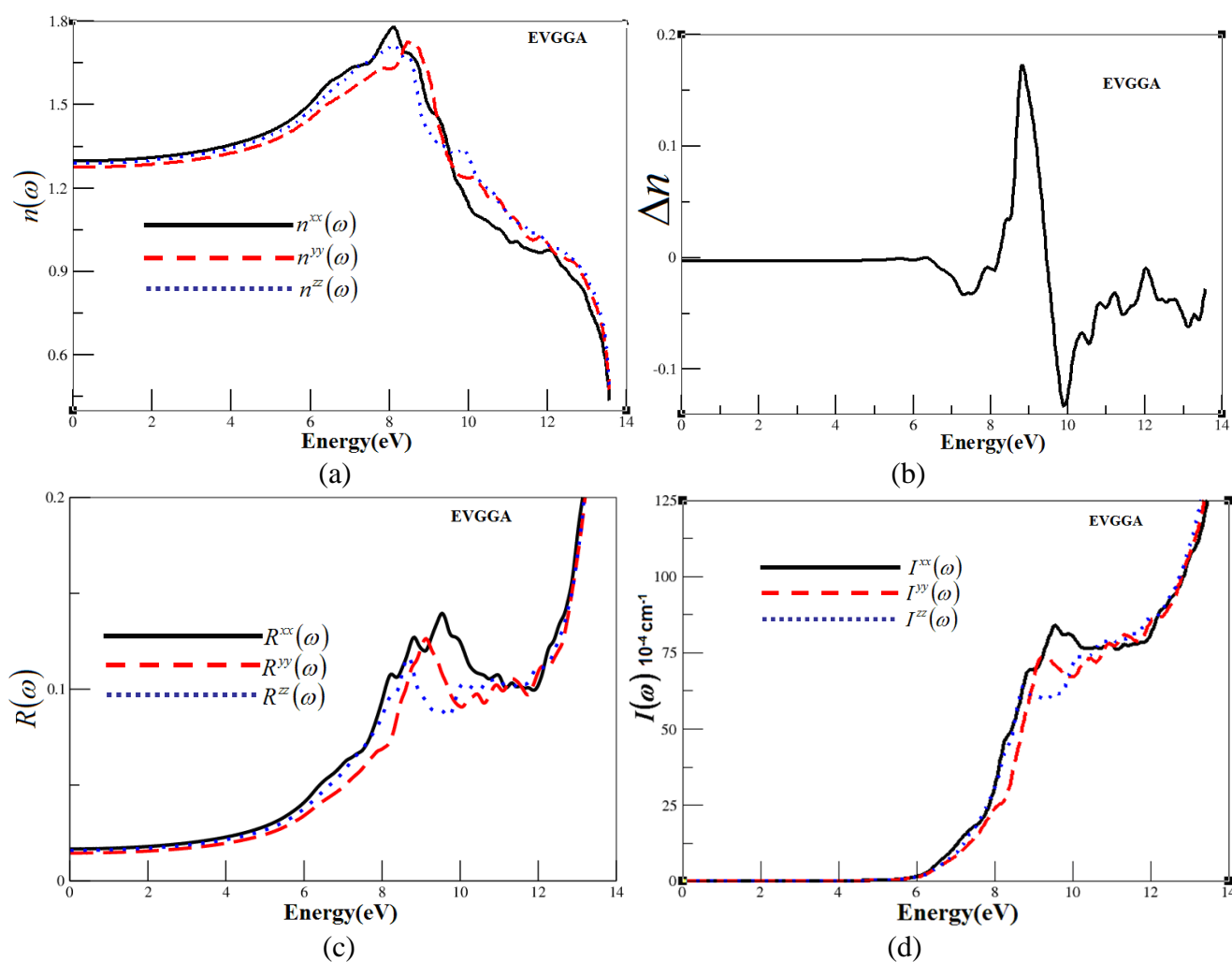


**Figure 6.** Calculated refractive index, reflectivity and absorption coefficient for  $\text{Rb}_2\text{Al}_2\text{B}_2\text{O}_7$  compound

Another important optical characteristic is the reflectivity spectrum, which is usually measured by experimentalists in order to determine all the other optical constants via Kramers–Kronig relations.

Fig. 6 shows the variation of the calculated refractive index and reflectivity (Fig. 6c) in relation with the energy of incident radiation. The reflectivity spectrum can be roughly characterized by three broad structures: the first between 6.0 and 8.0 eV, the second between 8.0 to 12.0 eV, and third situated around the 13.0 eV, respectively. There is no experimental data for the  $\text{Rb}_2\text{Al}_2\text{B}_2\text{O}_7$  reflectivity to be compared with our results. The interpretation of the reflectivity spectrum is closely related to the interpretation of the absorption spectrum, i.e. the same electronic transitions that cause the structures in the absorption spectrum (Fig. 6d) are responsible for the existence of the structures in the reflection spectrum. The absorption band, covering an energy range of 0.0–15.0 eV, shows a very intense absorption occurs between 9.0 and 13.5 eV.

#### 4. CONCLUSION

In this work we have presented comprehensive study of  $\text{Rb}_2\text{Al}_2\text{B}_2\text{O}_7$  compound using DFT based FP-LAPW method. Our objective was to investigate electronic structure, electronic charge density and optical properties of this material in the ultraviolet region up to 14.0 eV. The band gap is found to be indirect of about 4.156, 4.471 and 5.205 eV for LDA, GGA and EVGGA respectively. The top of the valence band and the bottom of the conduction band are mostly composed of the O s/p, Al s/p and the Rb s/p states, respectively. The electronic charge density maps (in the units of  $e/a.u.^3$ ) have been calculated along the (101) crystallographic plane. The bonding has a significant covalent character due to sharing of charge between O atoms. Moreover, the charge transfer occurs mainly from B and Al atoms towards O atom. The highest intensity peaks in the optical absorption spectrum of the  $\text{Rb}_2\text{Al}_2\text{B}_2\text{O}_7$  compound are caused by electronic transitions between exactly these states. We also calculated the effective mass of electrons, heavy holes and light hole.

The dielectric function, absorption coefficient, refractive index, birefringence and reflectivity spectrum are calculated for radiation up to 14 eV. Using the band structure, we have analyzed the interband contribution to the optical response functions. We show that O-p states and Rb-s and Al-s states play a major role in these optical transitions.

#### ACKNOWLEDGMENT

The result was developed within the CENTEM project, reg. no. CZ.1.05/2.1.00/03.0088, co-funded by the ERDF as part of the Ministry of Education, Youth and Sports OP RDI programme. School of Material Engineering, Malaysia University of Perlis, Malaysia.

#### References

1. C. Chen, Z. Lin, Z. Wang, *Appl. Phys. B* 80 (2005) 1-25.
2. Z.G. Hu, M. Yoshimura, Y. Mori, T. Sasaki, *J. Cryst. Growth* 275 (2005) 232-239.
3. A.S. Aleksandrovsky, A.M. Vyunishev, I.E. Shakhura, A.I. Zaitsev, A.V. Zamkov, A. V. *Phys. Rev. A* 78, 031802 (2008).
4. V. Petrov, M. Ghotbi, O. Kokabee, A. Esteban-Martin, F. Noack, A. Gaydardzhiev, I. Nikolov, P. Tzankov, I. Buchvarov, K. Miyata, A. Majchrowski, I.V. Kityk, F. Rotermund, E. Michalski, M. Ebrahim-Zadeh, *Laser Photon. Rev.* 4 (2010) 53-98.

5. R.A. Kumar, *J. Chem.* (2013) 154862.
6. N. Pylneva, V. Kosyakov, A. Yurkin, G. Bazarova, V. Atuchin, A. Kolesnikov, E. Trukhanov, C. Zilling, *Cryst. Res. Technol.* 36 (2001) 1377-1384.
7. A.P. Vasilenko, A.V. Kolesnikov, E.M. Trukhanov, N.A Pylneva, A.M. Yurkin, V.V. Atuchin, *J. Phys.: Condens. Matter* 15 (2003) 6801-6808.
8. E.G. Tsvetkov, G.G. Khranenko, V.P. Solntsev, *J. Cryst. Growth* 275 (2005) E2123-E2128.
9. D. Rajesh, M. Yoshimura, T. Eiro, Y. Mori, T. Sasaki, R. Jayavel, T. Kamimura, T. Katsura, T. Kojima, J. Nishimae, K. Yasui, *Opt. Mater.* 31 (2008) 461-463.
10. A. Kokh, N. Kononova, G. Mennerat, P. Villeval, S. Durst, D. Lupinski, V. Vlezko, K. Kokh, *J. Cryst. Growth* 312 (2010) 1774-1778.
11. V.V. Atuchin, L.D. Pokrovsky, V.G. Kesler, L.I. Isaenko, L.I. Gubenko, *J. Ceram. Process. Res.* 4 (2003) 84-87.
12. V.V. Atuchin, L.D. Pokrovsky, V.G. Kesler, N.Yu Maklakova, M. Yoshimura, N. Ushiyama, T. Matsui, K. Kamimura, Y. Mori, T. Sasaki, *Opt. Mater.* 23 (2003) 377-383.
13. V.V. Atuchin, T. Hasanov, V.G. Kesler, A.E. Kokh, L.D. Pokrovsky, *Opt. Mater.* 23 (2003) 385-392.
14. C. Cheng, X.X. Ding, F.J. Shi, Y. Cheng, X.T. Huang, S.R. Qi, C. Tang, *J. Cryst. Growth* 263 (2004) 600-604.
15. S.F. Xu, A.M. Chen, Z.M. Ni, S.F. Zhao, *Rare Metal Mater. Eng.* 39 (2010) 340-343.
16. W.C. Zhu, Q. Zhang, L. Xiang, S.L. Zhu, *Cryst Eng Comm* 13 (2011) 1654-1663.
17. Y.G. Ren, Y.C. Jia, N.N. Dong, L.L. Pang, Z.G. Wang, Q.M. Lu, F. Chen, *Opt. Lett.* 37 (2012) 244-246.
18. F. Chen, *Laser Photonics Rev.* 6 (2012) 622-640.
19. V.V. Atuchin, V.G. Kesler, A.I. Zaitsev, M.S. Molokeev, A.S. Aleksandrovsky, A.A. Kuzubov, N.Y. Ignatova, *J. Phys.: Condens. Matter* 25 (2013) 085503.
20. Z.-G. Hu, T. Higashiyama, M. Yoshimura, Y.K. Yap, Y. Mori, T. Sasaki, *Jpn. J. Appl. Phys.* 37 (1998) L1093.
21. Z.-G. Hu, T. Higashiyama, M. Yoshimura, Y. Mori, T. Sasaki, *J. Cryst. Growth* 212 (2000) 368.
22. N. Ye, W.R. Zeng, J. Jiang, B.C. Wu, C.T. Chen, B.H. Feng, X.L. Zhang, *J. Opt. Soc. Am. B* 17 (5) (2000) 764.
23. N. Umemura, M. Ando, K. Suzuki, E. Takaoka, K. Kato, Z.-G. Hu, M. Yoshimura, Y. Mori, T. Sasaki, *Appl. Opt.* 42 (15) (2003) 2716.
24. C.L. Liu, L.J. Liu, X. Zhang, L.R. Wang, G.L. Wang, C.T. Chen, *J. Cryst. Growth* 318 (2011) 618.
25. R.W. Smith, M.A. Kennard, M.J. Dudik, *Mater. Res. Bull.* 32 (6) (1997) 649.
26. M. He, X.L. Chen, H. Okudera, A. Simon, *Chem. Mater.* 17 (8) (2005) 2193.
27. Y.G. Wang, R.K. Li, *J. Solid State Chem.* 183 (2010) 1221.
28. Y.G. Wang, R.K. Li, *Opt. Mater.* 32 (2010) 1313.
29. Y.C. Yue, Z.X. Wu, Z.S. Lin, Z.-G. Hu, *Solid State Sci.* 13 (2011) 1172.
30. V.V. Atuchin, B.G. Bazarov, T.A. Gavrilova, V.G. Grossman, M.S. Molokeev, Z.G. Bazarova, *J. Alloys Compd.* 515 (2012) 119.
31. V.V. Atuchin et al. / *Materials Research Bulletin* 48 (2013) 929-934
32. P. Hohenberg, W. Kohn, *Phys. Rev.* 136 (1964) B864-B871; W. Kohn, L.J. Sham, *Phys. Rev.* 140 (1965) A1133-A1138.
33. O.K. Andersen, *Phys. Rev. B* 12 (1975) 3060-3083; D.J. Singh, *Plane Waves, Pseudopotentials and the LAPW Method*, Kluwer Academic, Dodrecht, 1994.
34. P. Blaha, K. Schwarz, G.K.H. Madsen, D. Kvasnicka, J. Luitz, *An Augmented Plane Waves + Local Orbital Program for Calculating Crystal Properties*, Institut Für Physikalische und Theoretische Chemie, Wien, Austria, 2001.
35. J. P. Perdew, A. Zunger, *Phys. Rev. B* 23, 5048 (1981).

36. J. P. Perdew, K. Burke, M. Ernzerhof, *Phys. Rev. Lett.* 77, 3865 (1996).
37. E. Engel, S. H. Vosko, *Phys. Rev.* B50, 10498 (1994).
38. A.D. Becke, E.R. Johnson, *J. Chem. Phys.* 124 (2006), 221101
39. M. Bass, E.W.V. Stryland, D.R. Willians, W.L. Woffe, *Handbook of Optics*, vol. 1, second ed., McGraw-Hill, New York, 1995.
40. L. Judith et. al. *Acta Cryst.*, E58, (2002) i85
41. B. Amin, R. Khenata, A. Bouhemadou, I. Ahmad, M. Maqbool. *Physica B* 407, (2012) 2588–2592
42. B. Amin, I. Ahmad, M. Maqbool, S. Goumri-Said, R. Ahmad. *J. Appl Phys.* 109 (2011) 023109
43. M. Maqbool, B. Amin, I. Ahmad. *J. Opt. Soc. Am. B.* 26(11) (2009) 2181-2184